



PERGAMON

International Journal of Solids and Structures 38 (2001) 1585–1603

INTERNATIONAL JOURNAL OF
**SOLIDS and
STRUCTURES**

www.elsevier.com/locate/ijsolstr

Lateral–torsional buckling of cantilevered elastically coupled composite strip- and I-beams

Dewey H. Hodges^{a,*}, David A. Peters^b

^a Georgia Institute of Technology, School of Aerospace Engineering, Atlanta, GA 30332-0150, USA

^b Department of Mechanical Engineering, Washington University, Saint Louis, MO 63130, USA

Received 10 December 1999; in revised form 21 March 2000

Abstract

The lateral–torsional buckling of composite strip- and I-beams is considered. The geometrically exact governing equations are simplified by consistently regarding certain configuration parameters as small. The assumption that these parameters are indeed small is equivalent to the assumption that the square of the maximum prebuckling cross-sectional rotation due to bending is small compared to unity. The analysis takes into account various refinements of previously published results, including the Vlasov effect, elastic coupling, the offset of the load from the centroid, and, of course, prebuckling deflections. The analysis is thereby reduced to a single fourth-order differential equation and boundary conditions, all of which are derivable from a corresponding energy expression. From the form of matched asymptotic expansions of the buckling mode when small parameters are ignored altogether, a single comparison function is found which gives the correct buckling load to within 1% for a wide range of the warping rigidity. Using this comparison function, a formula for the buckling load as a function of the small parameters of the problem is found and validated. With certain exceptions regarding the load offset parameter, the formula provides results which agree quite well with the numerical solution of the exact equations as long as all the small parameters remain small. However, the load offset parameter always appears in the governing equations as multiplied by a ratio of stiffnesses, which can become large, especially for composite I-beams. For this case, a special treatment is required. © 2001 Elsevier Science Ltd. All rights reserved.

Keywords: Structural stability; Elastic stability; Composite beams; Buckling; Asymptotic (or perturbation) method

1. Introduction

Elastic stability (or buckling) of beams, plates, and shells is one of the most important criteria in the design of any structure. Often, it is the critical design issue (even more than strength) in sizing certain structural elements. Because of this crucial role of elastic stability, it is extremely useful to have results of buckling analysis expressed in closed form, even if they are approximate, whenever possible for design

* Corresponding author. Tel.: +1-404-894-8302; fax: +1-404-894-9313.

E-mail address: dewey.hodges@aerospace.gatech.edu (D.H. Hodges).

analysis. Although such approximate analyses cannot replace an over-all elastic stability analysis of the entire structure, the ease of implementation and the physical insight that such forms give allows valuable design tradeoffs to be made in the preliminary design phase; and that can lead to significant improvements in cost and performance of the structural design. In this paper, we consider the lateral–torsional buckling of elastically coupled composite I-beams, and we look for closed-form approximate solutions that would be valuable in preliminary design.

The original work on the lateral–torsional stability of cantilevered beams goes back to the pioneering work of Michell (1899), Prandtl (1899), and Reissner (1904). Michell formulated the linear model for deep beams, and Prandtl and Reissner independently developed closed-form approximations for the buckling load that included some effects of bending prior to buckling. Hodges and Peters (1975) corrected some small errors in their earlier work. The corrected equations turned out to be simpler than the original ones, and Hodges and Peters used an asymptotic expansion to develop a closed-form buckling load formula that included the effect of bending prior to buckling in an asymptotically correct way. The method of asymptotic expansions was also used by Reissner (1979) to include the effect of shear deformations on the buckling of cantilever beams.

Since 1979, little further attention was given to the lateral buckling of cantilever beams until the advent of practical applications with composite materials. Work which attempts to address the potential of composites to improve the lateral–torsional stability of I-beams was presented by Pandey et al. (1995). The work was based on the composite I-beam theory of Bauld and Tzeng (1984). The theory of Bauld and Tzeng has been shown to fail in certain situations by a comparison with numerical solutions and with an asymptotically correct theory for composite I-beams developed by Volovoi et al. (1998). The purpose of the present work is to apply this more general, asymptotically correct theory of composite I-beams to the lateral–torsional stability of cantilevered beams at the same time giving heed to the effects of prebuckling deflections, offset of the applied load away from the centroid, and elastic coupling. The goal is to obtain an approximate, closed-form solution for the buckling load taking into account all of these phenomena.

2. Derivation of governing equations

Consider a thin-walled composite I-beam. When the flange length is zero, the beam has a thin rectangular cross-section (herein termed a “strip-beam”), so the treatment here is designed to treat both cases. Let the beam be cantilevered and loaded at its free end with a transverse dead load. The point of application for the load is in the plane of greatest flexural rigidity and at a distance \bar{e} above the centroidal axis, see Fig. 1.

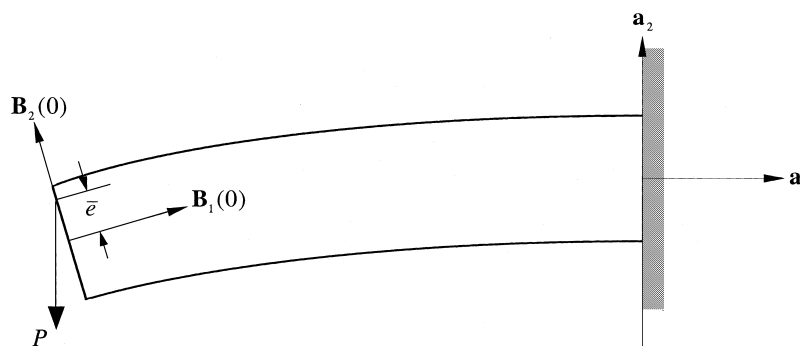


Fig. 1. Schematic of end-loaded cantilever.

The load is directed vertically downward, perpendicular to the undeformed beam axis and parallel to the plane of the beam's greatest flexural rigidity. In the figure, \mathbf{B}_1 , \mathbf{B}_2 , and \mathbf{B}_3 are unit vectors fixed in the cross-sectional frame. The beam is spanwise uniform and made of generally anisotropic materials, the only restriction being that the plane of greatest flexural rigidity is assumed to be a plane of symmetry for the beam geometry, material, and loading. This implies that prebuckling deflections of the beam axis occur in this plane and that in the prebuckling state there is no torsion. Thus, the cross-sectional frame rotates about $\mathbf{a}_3 = \mathbf{B}_3$ by the angle θ_3 .

Ignoring the stretching of the beam, this means that there is elastic coupling only between torsion and bending about the weak flexural axis. Asymptotically exact formulae for the cross-sectional stiffness constants of thin-walled anisotropic strip- and I-beams can be found in Volovoi et al. (1998). The only difference in the two cases is that the Vlasov term (see below) is absent in the strip-beam case, but very important for the I-beam. For the present analysis, the constitutive law is only needed for the moment stress resultants. Let x_1 be the beam axial coordinate and x_2 and x_3 be its cross-sectional principal axes for bending, it is of the form

$$\begin{aligned} M_1 &= D_{11}K_1 + D_{12}K_2, \\ M_2 &= D_{12}K_1 + D_{22}K_2, \\ M_3 &= D_{33}K_3, \\ Q_1 &= D_{44}K'_1, \end{aligned} \tag{1}$$

where ()' denotes the derivative with respect to x_1 . Here and throughout this paper, Latin indices vary from 1 to 3, and Greek ones from 2 to 3. It is noted that $\mathbf{B}'_i = \mathbf{K} \times \mathbf{B}_i$ with $K_i = \mathbf{K} \cdot \mathbf{B}_i$. Thus, K_1 is the elastic twist per unit length, and K_x are the elastic bending curvatures. The cross-sectional moment stress resultant is \mathbf{M} , with $M_i = \mathbf{M} \cdot \mathbf{B}_i$, and Q_1 is the bi-moment. For isotropic beams $D_{12} = 0$; D_{11} , D_{22} , D_{33} , and D_{44} are usually written as GJ , EI_2 , EI_3 , and $E\Gamma$ with G as the shear modulus, E as Young's modulus, J as the Saint-Venant torsion constant, I_x as area moments of inertia, and Γ as the Vlasov constant (sometimes called warping rigidity). The only difference between the models for the two types of beams is the presence (absence) of the stiffness constant D_{44} in the case of the I-beam (strip-beam).

The present analysis will be based on the geometrically exact equilibrium equations of classical¹ beam theory as augmented with the Vlasov effect. One can write these equations in a compact form as demonstrated in Hodges (1990). These equations are easily augmented with the effect of K'_1 in the strain energy (the so-called Vlasov effect) to yield

$$\begin{aligned} F'_1 - F_2K_3 + F_3K_2 &= 0, \\ F'_2 - F_3K_1 + F_1K_3 &= 0, \\ F'_3 - F_1K_2 + F_2K_1 &= 0, \\ M'_1 - M_2K_3 + M_3K_2 - Q'_1 &= 0, \\ M'_2 - M_3K_1 + M_1K_3 - (1 + \epsilon)F_3 - K_3Q'_1 &= 0, \\ M'_3 - M_1K_2 + M_2K_1 + (1 + \epsilon)F_2 + K_2Q'_1 &= 0, \end{aligned} \tag{2}$$

where the cross-sectional stress resultant is \mathbf{F} , and $F_i = \mathbf{F} \cdot \mathbf{B}_i$. For small-strain analysis, it is permissible to drop the stretching strain ϵ compared to unity in the last two equations.

¹ The term "classical" is used to refer to the fact that transverse shear deformation is neglected.

For lateral–torsional buckling analysis, one can let

$$\begin{aligned} K_i &= \bar{K}_i + \hat{K}_i, \\ F_i &= \bar{F}_i + \hat{F}_i, \\ M_i &= \bar{M}_i + \hat{M}_i, \\ Q_1 &= \bar{Q}_1 + \hat{Q}_1, \end{aligned} \quad (3)$$

where the ($\hat{\quad}$) quantities are regarded as infinitesimal, and write two sets of equations from the above. The first set, which contains no ($\hat{\quad}$) quantities, can be described as the prebuckling equations of equilibrium. The second set which is linear in the ($\hat{\quad}$) quantities is the set of equations which govern the stability.

The prebuckling equilibrium equations only involve F_1 , F_2 , and M_3 and are given by

$$\begin{aligned} \bar{F}'_1 - \bar{F}_2 \bar{K}_3 &= 0, \\ \bar{F}'_2 + \bar{F}_1 \bar{K}_3 &= 0, \\ \bar{M}'_3 + \bar{F}_2 &= 0, \end{aligned} \quad (4)$$

where $\bar{K}_3 = \bar{\theta}'_3$. Letting $\bar{F}_1 = P \sin \bar{\theta}_3$ and $\bar{F}_2 = P \cos \bar{\theta}_3$, one can reduce the prebuckling equations to one equation:

$$D_{33} \bar{\theta}''_3 + P \cos \bar{\theta}_3 = 0 \quad (5)$$

subject to boundary conditions $\bar{\theta}_3(l) = 0$ and $\bar{M}_3(0) = -\bar{e}P \sin \bar{\theta}_3(0)$.

The required perturbation equations for buckling analysis can be written as

$$\hat{F}'_3 - P \sin \bar{\theta}_3 \hat{K}_2 + P \cos \bar{\theta}_3 \hat{K}_1 = 0, \quad (6a)$$

$$\hat{M}'_1 - \bar{K}_3 \hat{M}_2 + \bar{M}_3 \hat{K}_2 - \hat{Q}'_1 = 0, \quad (6b)$$

$$\hat{M}'_2 - \bar{M}_3 \hat{K}_1 + \bar{K}_3 \hat{M}_1 - \hat{F}_3 - \bar{K}_3 \hat{Q}'_1 = 0, \quad (6c)$$

subject to boundary conditions $\hat{F}_3(l) = 0$, $\hat{K}_1(l) = 0$, $\hat{K}'_1(0) = 0$, $\hat{M}_1(0) - \hat{Q}'_1(0) - \bar{e} \hat{F}_3(0) = 0$, and $\hat{M}_2(0) = 0$.

The exact solution to these equations is unknown. What is of interest here is to find an approximate closed-form solution for the buckling load. The approach of Hodges and Peters (1975) was shown therein to provide excellent accuracy for the buckling load and the effects of a variety of secondary phenomena.

To undertake this approach in the present context, one must introduce a set of small parameters. First, the square of the prebuckling rotation is assumed to be small compared to unity, so that $\bar{\theta}_3^2 \ll 1$. Thus, the prebuckling rotation equation, Eq. (5), can be simplified to

$$D_{33} \bar{\theta}''_3 + P = 0. \quad (7)$$

Using arguments similar to those of Hodges and Peters (1975), one can easily show that the following small parameters are all of the same order:

$$\begin{aligned} \max(\bar{\theta}_3) &= \frac{Pl^2}{D_{33}}, \\ e &= \frac{\bar{e}}{l}, \\ A &= \frac{D_{11}}{D_{33}}, \\ B &= \frac{D_{22}}{D_{33}}. \end{aligned} \quad (8)$$

Thus, one can solve Eq. (7) to obtain

$$\bar{\theta}_3 = \frac{P(l^2 - x_1^2)}{D_{33}}. \tag{9}$$

It should be noted that Hodges and Peters (1975) did not consider the parameter e . It is noted below that there are circumstances under which one should not assume that e is small.

Introducing κ such that $D_{12} = \kappa\sqrt{D_{11}D_{22}}$ and γ such that

$$D_{44} = \gamma D_{11}l^2 = \gamma AD_{33}l^2, \tag{10}$$

one can write the entire constitutive law in terms of D_{33} and the nondimensional parameters A , B , κ , and γ . Following Hodges and Peters (1975), we note that the combination of Eq. (6b) plus $\bar{\theta}_3$ times Eq. (6c) yields an equation which, when small terms are consistently neglected, is a perfect differential of

$$k + BK_2 + AK_1\bar{\theta}_3 + \sqrt{A}\sqrt{B}\kappa(K_1 + K_2\bar{\theta}_3) + \frac{F_3\bar{\theta}_3'}{P} - Al^2\gamma\bar{\theta}_3K_1'' = 0, \tag{11}$$

where k is an arbitrary constant to be determined later. This equation can be solved along with Eq. (6a) for \hat{K}_1 and \hat{K}_2 . When small terms are discarded consistently, one obtains

$$\begin{aligned} \hat{K}_1 &= -\phi' + \frac{\bar{\theta}_3(\sqrt{A}\sqrt{B}\kappa\phi' - \phi\bar{\theta}_3')}{B}, \\ \hat{K}_2 &= \frac{-Bk + \sqrt{AB}^{3/2}\kappa\phi' - B\phi\bar{\theta}_3' + \sqrt{A}\bar{\theta}_3[\sqrt{AB}(1 - 2\kappa^2)\phi' + 2\sqrt{B}\kappa\phi\bar{\theta}_3' - \sqrt{AB}l^2\gamma\phi''']}{B^2}, \end{aligned} \tag{12}$$

where the nondimensional perturbation out-of-plane shear force $\phi = \hat{F}_3/P$. Thus, the \hat{M}_1 equation, Eq. (6b), and all the boundary conditions can now be expressed completely in terms of ϕ and its derivatives with respect to x_1 .

To facilitate the writing of this equation, we introduce a nondimensional buckling load β such that $P = \beta\sqrt{D_{11}D_{22}}/l^2 = \beta\sqrt{AB}D_{33}/l^2$ and a nondimensional axial coordinate x such that $lx = x_1$. The constant k can be found to be

$$k = \frac{A^{3/2}\sqrt{B}\beta[(1 - \kappa^2)\phi'(0) - \gamma\phi'''(0)]}{2}, \tag{13}$$

where the prime now indicates a derivative with respect to x . However, use of the boundary conditions leads to homogeneous equations without boundary values of the unknown in them. It turns out that the boundary conditions must be multiplied by appropriate constants in order to make them variationally consistent. The details of this operation are straightforward and not given here. The resulting equation is

$$\begin{aligned} &\gamma[1 - A(1 - x^2)\beta\kappa]\phi'''' + 4Ax\beta\gamma\kappa\phi''' - [1 + \frac{3}{2}A(1 - 3x^2)\beta^2\gamma - A\beta(1 - x^2 + 3\gamma)\kappa - \kappa^2 \\ &\quad + A(1 - x^2)\beta\kappa^3]\phi'' + Ax\beta(9\beta\gamma - 2\kappa + 2\kappa^3)\phi' - \beta\{(1 - B)x^2\beta - \kappa - A\beta[3\gamma + x^2(1 - x^2)\beta\kappa \\ &\quad + (1 - 3x^2)(\frac{1}{2} - \kappa^2)]\}\phi = 0, \end{aligned} \tag{14}$$

and the boundary conditions are

$$\begin{aligned}\phi(1) &= \phi'(1) = 0, \\ \gamma \left[(1 - A\beta\kappa)\phi''(0) - \frac{A\beta^2\phi(0)}{2} \right] &= 0, \\ \gamma(1 - A\beta\kappa)\phi'''(0) - [(1 - \kappa^2)(1 - A\beta\kappa) - A\beta\gamma(\kappa - \beta)]\phi'(0) - \frac{\sqrt{Be}\beta\phi(0)}{\sqrt{A}} &= 0.\end{aligned}\tag{15}$$

For stability analysis, it is convenient to work in terms of an energy functional in terms of ϕ and its derivatives and boundary values. This functional can be shown to be of the form

$$L = \frac{1}{2} \int_0^1 (L_0\phi^2 + L_1\phi'^2 + L_2\phi''^2) dx + \frac{A\beta^2\gamma\phi(0)\phi'(0)}{2} - \frac{\sqrt{Be}\beta\phi^2(0)}{2\sqrt{A}},\tag{16}$$

where

$$\begin{aligned}L_0 &= -\beta[(1 - B)x^2\beta - \kappa] + \frac{A\beta^2}{2} [1 + 6\gamma - 2x^4\beta\kappa - 2\kappa^2 - x^2(3 - 2\beta\kappa - 6\kappa^2)], \\ L_1 &= 1 + 2A\beta\gamma\kappa - \kappa^2 - A\beta\left[\frac{3}{2}(3x^2 - 1)\beta\gamma + \kappa(1 - x^2 + 3\gamma - \kappa^2 + x^2\kappa^2)\right], \\ L_2 &= \gamma[1 - A(1 - x^2)\beta\kappa].\end{aligned}\tag{17}$$

The above differential equation, boundary conditions, and functional reduce to the corresponding expressions given by Hodges and Peters (1975) when $\gamma = e = \kappa = 0$.

For both the strip- and I-beam cases, the load offset parameter e is multiplied by $\sqrt{B/A}$ in its only appearance in the formulation. Somewhat complicating the procedure from here on, is the fact that this quantity may be large under certain circumstances, thus magnifying the influence of the e parameter. In such cases, the assumption that e is small ought to be relaxed. Such cases will be considered below in each of the two cases.

3. Approximate solution

3.1. Case of zero warping rigidity

For thin beams having rectangular cross-sections (i.e., strip-beams), the Vlasov effect may be ignored even for anisotropic beams according to Volovoi et al. (1998). For the case of zero warping rigidity, i.e., $\gamma = 0$, the above equations and energy functional are greatly simplified. The main reason for the simplification mathematically is that the order of the governing equations and number of boundary conditions are reduced. The differential equation becomes

$$\begin{aligned}[1 - A\beta\kappa(1 - x^2)](1 - \kappa^2)\phi'' + 2A\beta\kappa x(1 - \kappa^2)\phi' + \beta \left\{ (1 - B)x^2\beta - \kappa - A\beta \left[x^2(1 - x^2)\beta\kappa \right. \right. \\ \left. \left. + (1 - 3x^2) \left(\frac{1}{2} - \kappa^2 \right) \right] \right\} \phi = 0,\end{aligned}\tag{18}$$

and the boundary conditions are

$$\begin{aligned}\phi(1) &= 0, \\ (1 - \kappa^2)(1 - A\beta\kappa)\phi'(0) + \frac{\sqrt{B}e\beta\phi(0)}{\sqrt{A}} &= 0.\end{aligned}\tag{19}$$

The solution to this boundary-value problem is not known to the authors. However, using the solution to the case $A = B = e = \kappa = 0$ to obtain an accurate comparison function, as done by Hodges and Peters (1975), one obtains a useful result. To do so, one notes that the solution of the simplified equation is $\phi = \psi$, where

$$\psi = \sqrt{x}J_{-\frac{1}{4}}\left(\frac{4.0126x^2}{2}\right),\tag{20}$$

where the factor 4.0126 is the smallest positive zero of the Bessel function $J_{-\frac{1}{4}}(\beta/2)$. Using this function in the energy allows one to solve for β , given by

$$\beta = 4.0126\left(1 + 0.642365A + \frac{B}{2} - 1.02543\sqrt{\frac{B}{A}}e\right) + 2.78473\kappa - 1.04\kappa^2,\tag{21}$$

where κ^2 is taken to be of the same order as A , B , and e . This expansion in κ is valid for κ up to about 0.5, which is sufficiently large for most purposes. One can use the expansion to find the buckling load of uniform strip-beams.

Unfortunately, when $e\sqrt{B/A}$ is not small of the same order as A , the above expansion breaks down. For anisotropic strip-beams, for example, one can have the effective ratio of extension modulus to shear modulus (E/G) quite large. This would tend to magnify the influence of the load offset. The solution to the case in which $e\sqrt{B/A} \neq 0$, but where otherwise $A = B = \kappa = 0$ is

$$\psi = \sqrt{x}\left[c_1J_{-\frac{1}{4}}\left(\frac{x^2\beta}{2}\right) + c_2J_{\frac{1}{4}}\left(\frac{x^2\beta}{2}\right)\right]\tag{22}$$

subject to the boundary conditions

$$\begin{aligned}\phi(1) &= 0, \\ \phi'(0) + \frac{\sqrt{B}e\beta\phi(0)}{\sqrt{A}} &= 0,\end{aligned}\tag{23}$$

which leads to a characteristic equation that can be solved numerically for β given any value of $e\sqrt{B/A}$. A plot of the solution is shown in Fig. 2. Indeed, in the limit of large and positive $e\sqrt{B/A}$, the result approaches the case of applying a downward compressive load at the end of a long, rigid rod extending upward from the beam axis (instead of from within the beam cross-section). This buckling load β clearly approaches zero as the length of the rigid rod increases. On the other hand, when $e\sqrt{B/A}$ is large and negative, the buckling load approaches that for a downward tensile load applied at the end of a long, rigid rod extending downward (i.e., in the direction of the load). In this case, the buckling load approaches that for the case of $\phi(0) = 0$, for which $\beta = 5.56178$, the smallest positive zero of $J_{\frac{1}{4}}(\beta/2)$. Obviously no linear function of e can capture this behavior outside of a small range near $e\sqrt{B/A} = 0$. Eq. (21) is then not valid in the cases when $e\sqrt{B/A}$ is not small, but it can serve to indicate the trend of β versus e . One could develop

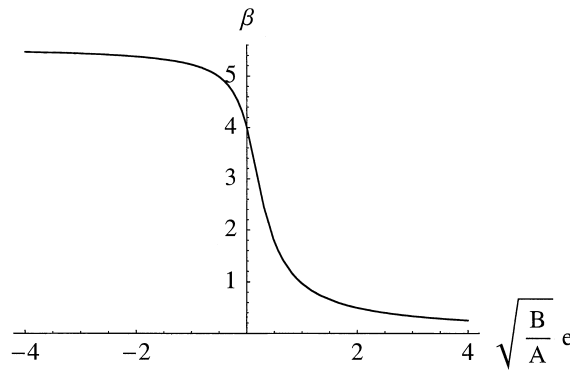


Fig. 2. Plot of β versus $e\sqrt{\frac{B}{A}}$.

a comparison function which contains e as a parameter, but the resulting buckling load formulae would be very complex.

3.2. Case of nonzero warping rigidity

The case of nonzero warping rigidity is far more difficult. The governing equations and boundary conditions with all secondary effects set to zero are

$$\begin{aligned} \gamma\phi'''' - \phi'' - x^2\beta^2\phi &= 0, \\ \phi(1) = \phi'(1) = \phi''(0) = \gamma\phi'''(0) - \phi'(0) &= 0. \end{aligned} \tag{24}$$

Other than an infinite series solution, results of which are presented in Timoshenko and Gere (1961), the solution to this deceptively simple-looking boundary-value problem is not known to the authors. Without a one-term solution which has an explicit behavior in γ , one has no exact “zeroth-order” solution to use as the assumed mode in the energy to find the buckling load in the presence of the small parameters A , B , e , and κ . The only alternative seems to be some kind of approximate comparison function.

In Eq. (24), the parameter, γ , can vary from being small compared to unity to being considerably larger than unity. In order to obtain a better understanding of the behavior of the equation, it is interesting to first look at the limiting behaviors for cases of γ small and γ large. A natural means of doing this is the method of matched asymptotic expansions. In that method, the buckling load parameter, β , must be expanded in some selected powers of γ as must the solution, ϕ , itself. Furthermore, there must be an expansion of the independent variable, x , in terms of powers of γ at the fixed and free ends (the boundary layers) in order to capture the correct limiting behavior. The solutions in the boundary layers (inner solutions) must be matched (as the inner variables become large) to the general solution away from the ends (outer expansion) as the outer variable approaches either end. This yields a unique solution for the buckling load and the buckling mode shape. As the term with γ multiplies ϕ'''' , and the next highest derivative is ϕ'' , all expansions for small γ must be done in powers of $\gamma^{1/2}$ in order to allow the inner and outer solutions to be matched. As it turns out, only the fixed end ($x = 1$) has a boundary layer that affects the outer solution and buckling load to order $\gamma^{1/2}$ or γ^1 . The resultant expansion shows that the boundary layer dies out into the outer solution as $\exp[-(1-x)/\gamma^{1/2}]$. The next term in the outer expansion (and the next term in the expression for the approximate buckling load) can then be found by solving a nonhomogeneous, second-order equation for the

outer solution. This involves integrals of the Bessel functions that are rather involved. For our purposes here, it is enough to know how the fixed-end boundary layer behaves and, particularly, how it decays into the outer region.

The large γ solution can be written in terms of confluent, hypergeometric functions. Since no derivatives are lost as γ becomes large, there are no boundary layers or matching required in that case. One can do a straightforward expansion in terms of the small parameter, $1/\gamma$. The first expansion term in that solution involves fairly complicated integrals of the hypergeometric functions and is not tractable in closed form. Nevertheless, the fact that there are no boundary layers in that solution, indicates that an approximation for the entire mode, fairly accurate at all values of γ , might be constructed from simple polynomials plus the crucial boundary layer terms. In contrast to the asymptotic expansions, in which boundary conditions are satisfied only to the order of the expansion that is taken, here, we use the exponential decay term for the fixed end and add the simplest possible polynomial that will match the other boundary conditions exactly. We expect that this comparison function will provide accurate results. Whether or not this expectation is realized can only be determined by comparison with numerical solutions to the exact equations.

Taking a cubic polynomial along with the exponential, one finds the simplest comparison function of that form (i.e., one which satisfies all the boundary conditions in Eq. (24)) to be

$$\theta = (1-x)^2(1+2x-6\gamma)e^{-1/\sqrt{\gamma}} + 6e^{-(1-x)/\sqrt{\gamma}}\gamma(1+2\gamma) + 2\sqrt{\gamma}[1-x^3-3\sqrt{\gamma}+6(1-x)\gamma-6\gamma^{3/2}]. \quad (25)$$

The use of $\phi = \theta$ in the energy functional which corresponds to Eq. (24) will give an approximate closed-form expression for the nondimensional buckling load β . This energy functional is simply

$$\beta^2 = \frac{\int_0^1 (\phi'^2 + \gamma\phi''^2) dx}{\int_0^1 x^2\phi^2 dx}. \quad (26)$$

The accuracy of this predicted buckling load as a function of γ can be regarded as a measure of how well θ performs as a one-term approximation of the actual buckling mode ϕ . The nondimensional buckling load can be written as $\beta = \beta_0$, where

$$\beta_0 = \sqrt{\frac{\eta_0 + \eta_1 e^{-1/\sqrt{\gamma}} + \eta_2 e^{-2/\sqrt{\gamma}}}{\delta_0 + \delta_1 e^{-1/\sqrt{\gamma}} + \delta_2 e^{-2/\sqrt{\gamma}}}}, \quad (27)$$

where

$$\begin{aligned} \eta_0 &= 1512\gamma(3 - 15\sqrt{\gamma} + 40\gamma - 60\gamma^{3/2} + 60\gamma^2 - 60\gamma^{5/2}), \\ \eta_1 &= 756\sqrt{\gamma}\{3 - 10\gamma[1 - 12\gamma(1 + 2\gamma)]\}, \\ \eta_2 &= 756\{1 - 10\gamma^{3/2}[3 + 4(2\sqrt{\gamma} + 3\gamma + 3\gamma^{3/2} + 3\gamma^2)]\}, \\ \delta_0 &= 2\gamma[140 - 9\sqrt{\gamma}(140 - 520\sqrt{\gamma} + 70\gamma + 8862\gamma^{3/2} - 47,355\gamma^2 \\ &\quad + 131,880\gamma^{5/2} - 215,460\gamma^3 + 224,280\gamma^{7/2} - 243,180\gamma^4)], \\ \delta_1 &= \sqrt{\gamma}[133 - 18(28\sqrt{\gamma} - 3\gamma - 28\gamma^{3/2} - 2436\gamma^2 + 21,672\gamma^{5/2} \\ &\quad - 75,600\gamma^3 + 124,320\gamma^{7/2} + 40,320\gamma^4 + 161,280\gamma^{9/2} + 362,880\gamma^5)], \\ \delta_2 &= 19 - 18\gamma\{7 - 3\gamma\{4 - 35\sqrt{\gamma}(1 + 2\gamma)[8 - 3\gamma(111 + 416\sqrt{\gamma} + 190\gamma)]\}\}. \end{aligned} \quad (28)$$

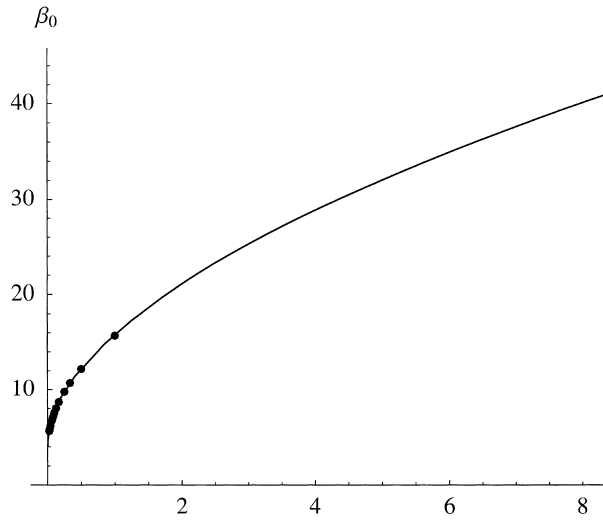


Fig. 3. β_0 versus γ compared with exact solution (symbols) from Timoshenko and Gere (1961).

Indeed, one finds an error of less than 1% over a wide range of γ , certainly within an acceptable range of error for design purposes. In Fig. 3, the value of β_0 is plotted versus γ over a wide range. The symbols are the exact solutions at discrete values of γ taken from Table 6-3 of Timoshenko and Gere (1961), Page 259. Notice that the symbols are on top of the curve, to within plotting accuracy, over the whole range of γ shown. Moreover, for $\gamma \rightarrow 0$, the relative error from Eq. (27) is only 0.3% off the exact solution of 4.0126. For $\gamma \rightarrow \infty$, the limiting value of β_0 is 13.9473γ , only about 1% off the exact value of 13.8058γ .

When $\phi = \theta$ is substituted into the energy, Eq. (16), one can easily solve for β in terms of γ and the small parameters A, B, e , and κ . This is most easily accomplished by the use of a perturbation expansion in terms of the small parameters, keeping terms up through first order in A, B , and e , and through second order in κ as in Eq. (21). This equation is expressible in the form

$$\beta = \left(1 + \frac{B}{2}\right)\beta_0 + A\beta_A + e\sqrt{\frac{B}{A}}\beta_e + \kappa\beta_1 + \kappa^2\beta_2, \tag{29}$$

where

$$\begin{aligned} \beta_A &= \frac{9\sqrt{21}\sqrt{a_0 + a_1e^{-1/\sqrt{\gamma}} + a_2e^{-2/\sqrt{\gamma}}}(b_0 + b_1e^{-1/\sqrt{\gamma}} + b_2e^{-2/\sqrt{\gamma}})}{2(c_0 + c_1e^{-1/\sqrt{\gamma}} + c_2e^{-2/\sqrt{\gamma}})^{3/2}}, \\ \beta_e &= -315 \frac{[2\sqrt{\gamma} - 6\gamma + 12\gamma^{3/2} - 12\gamma^2 + (1 + 12\gamma^2)e^{-1/\sqrt{\gamma}}]^2}{\alpha_0 + \alpha_1e^{-1/\sqrt{\gamma}} + \alpha_2e^{-2/\sqrt{\gamma}}}, \\ \beta_1 &= \frac{d_0 + d_1e^{-1/\sqrt{\gamma}} + d_2e^{-2/\sqrt{\gamma}}}{k_0 + k_1e^{-1/\sqrt{\gamma}} + k_2e^{-2/\sqrt{\gamma}}}, \\ \beta_2 &= \frac{3\sqrt{21}(p_0 + p_1e^{-1/\sqrt{\gamma}} + p_2e^{-2/\sqrt{\gamma}})^2(q_0 + q_1e^{-1/\sqrt{\gamma}} + q_2e^{-2/\sqrt{\gamma}} + q_3e^{-3/\sqrt{\gamma}} + q_4e^{-4/\sqrt{\gamma}})}{28\sqrt{r_0 + r_1e^{-1/\sqrt{\gamma}} + r_2e^{-2/\sqrt{\gamma}}}(s_0 + s_1e^{-1/\sqrt{\gamma}} + s_2e^{-2/\sqrt{\gamma}})^{3/2}}, \end{aligned} \tag{30}$$

and where

$$\begin{aligned}
 a_0 &= 2\gamma(3 - 15\sqrt{\gamma} + 40\gamma - 60\gamma^{3/2} + 60\gamma^2 - 60\gamma^{5/2}), \\
 a_1 &= \sqrt{\gamma}\{3 + 10\gamma[-1 + 12\gamma(1 + 2\gamma)]\}, \\
 a_2 &= 1 - 10\gamma^{3/2}[3 + 4(2\sqrt{\gamma} + 3\gamma + 3\gamma^{3/2} + 3\gamma^2)], \\
 b_0 &= 4\gamma[65 - 9\sqrt{\gamma}(35 - 22\sqrt{\gamma} - 770\gamma + 5880\gamma^{3/2} - 24,360\gamma^2 \\
 &\quad + 62,160\gamma^{5/2} - 95,760\gamma^3 + 100,800\gamma^{7/2} - 100,800\gamma^4)], \\
 b_1 &= \sqrt{\gamma}[257 - 6(126\sqrt{\gamma} - 247\gamma + 924\gamma^{3/2} - 10,584\gamma^2 + 66,864\gamma^{5/2} \\
 &\quad - 226,800\gamma^3 + 312,480\gamma^{7/2} + 10,080\gamma^4 + 362,880\gamma^{9/2} + 846,720\gamma^5)], \\
 b_2 &= 59 + 30\gamma\{1 - 24\gamma[1 + 42\sqrt{\gamma}(1 + 2\gamma)(1 + 3\sqrt{\gamma} - 10\gamma - 60\gamma^{3/2} - 24\gamma^2)]\}, \\
 c_0 &= 2\gamma[140 - 9\sqrt{\gamma}(140 - 520\sqrt{\gamma} + 70\gamma + 8862\gamma^{3/2} - 47,355\gamma^2 \\
 &\quad + 131,880\gamma^{5/2} - 215,460\gamma^3 + 224,280\gamma^{7/2} - 243,180\gamma^4)], \\
 c_1 &= \sqrt{\gamma}[133 - 18(28\sqrt{\gamma} - 3\gamma - 28\gamma^{3/2} - 2436\gamma^2 + 21,672\gamma^{5/2} - 75,600\gamma^3 \\
 &\quad + 124,320\gamma^{7/2} + 40,320\gamma^4 + 161,280\gamma^{9/2} + 362,880\gamma^5)], \\
 c_2 &= 19 - 18\gamma\{7 - 3\gamma\{4 - 35\sqrt{\gamma}(1 + 2\gamma)[8 - 3\gamma(111 + 416\sqrt{\gamma} + 190\gamma)]\}\},
 \end{aligned} \tag{31}$$

$$\begin{aligned}
 \alpha_0 &= 2\gamma[140 + 9\sqrt{\gamma}(-140 + 520\sqrt{\gamma} - 70\gamma - 8862\gamma^{3/2} + 47,355\gamma^2 \\
 &\quad - 131,880\gamma^{5/2} + 215,460\gamma^3 - 224,280\gamma^{7/2} + 243,180\gamma^4)], \\
 \alpha_1 &= \sqrt{\gamma}[133 - 18(28\sqrt{\gamma} - 3\gamma - 28\gamma^{3/2} - 2436\gamma^2 + 21,672\gamma^{5/2} \\
 &\quad - 75,600\gamma^3 + 124,320\gamma^{7/2} + 40,320\gamma^4 + 161,280\gamma^{9/2} + 362,880\gamma^5)], \\
 \alpha_2 &= 19 - 18\gamma\{7 - 3\gamma\{4 - 35\sqrt{\gamma}(1 + 2\gamma)[8 - 3\gamma(111 + 416\sqrt{\gamma} + 190\gamma)]\}\},
 \end{aligned} \tag{32}$$

$$\begin{aligned}
 d_0 &= 810\gamma - 5670\gamma^{3/2} + 18,144\gamma^2 - 28,350\gamma^{5/2} \\
 &\quad + 15,120\gamma^3 + 22,680\gamma^{7/2} - 45,360\gamma^4 + 113,400\gamma^{9/2}, \\
 d_1 &= 585\sqrt{\gamma} - 1890\gamma + 252\gamma^{3/2} - 3780\gamma^2 \\
 &\quad + 34,020\gamma^{5/2} - 90,720\gamma^3 - 181,440\gamma^4 - 181,440\gamma^{9/2}, \\
 d_2 &= 117 - 1008\gamma - 3780\gamma^{3/2} + 2268\gamma^2 + 32,130\gamma^{5/2} + 90,720\gamma^3 \\
 &\quad + 113,400\gamma^{7/2} + 181,440\gamma^4 + 68,040\gamma^{9/2}, \\
 k_0 &= 280\gamma - 2520\gamma^{3/2} + 9360\gamma^2 - 1260\gamma^{5/2} - 159,516\gamma^3 + 852,390\gamma^{7/2} \\
 &\quad - 2,373,840\gamma^4 + 3,878,280\gamma^{9/2} - 4,037,040\gamma^5 + 4,377,240\gamma^{11/2}, \\
 k_1 &= 133\sqrt{\gamma} - 504\gamma + 54\gamma^{3/2} + 504\gamma^2 + 43,848\gamma^{5/2} - 390,096\gamma^3 \\
 &\quad + 1,360,800\gamma^{7/2} - 2,237,760\gamma^4 - 725,760\gamma^{9/2} - 2,903,040\gamma^5 - 6,531,840\gamma^{11/2}, \\
 k_2 &= 19 - 126\gamma + 216\gamma^2 - 15,120\gamma^{5/2} + 599,130\gamma^{7/2} + 2,358,720\gamma^4 \\
 &\quad + 2,336,040\gamma^{9/2} + 4,717,440\gamma^5 + 2,154,600\gamma^{11/2},
 \end{aligned} \tag{33}$$

and

$$\begin{aligned}
 p_0 &= 6\gamma[15 - 7\sqrt{\gamma}(15 - 48\sqrt{\gamma} + 75\gamma - 40\gamma^{3/2} - 60\gamma^2 + 120\gamma^{5/2} - 300\gamma^3)], \\
 p_1 &= \sqrt{\gamma}[65 - 14\sqrt{\gamma}(15 - 2\sqrt{\gamma} + 30\gamma - 270\gamma^{3/2} + 720\gamma^2 + 1440\gamma^3 + 1440\gamma^{7/2})], \\
 p_2 &= 13 - 14\gamma[8 + 3\sqrt{\gamma}(10 - 6\sqrt{\gamma} - 85\gamma - 240\gamma^{3/2} - 300\gamma^2 - 480\gamma^{5/2} - 180\gamma^3)],
 \end{aligned} \tag{34}$$

$$\begin{aligned}
q_0 &= -56\gamma^2(6 - 45\sqrt{\gamma} + 160\gamma - 300\gamma^{3/2} + 360\gamma^2 - 420\gamma^{5/2})[140 - 9\sqrt{\gamma}(140 \\
&\quad - 520\sqrt{\gamma} + 70\gamma + 8862\gamma^{3/2} - 47,355\gamma^2 + 131,880\gamma^{5/2} - 215,460\gamma^3 \\
&\quad + 224,280\gamma^{7/2} - 243,180\gamma^4)], \\
q_1 &= -28\gamma^{3/2}\{1638 - \sqrt{\gamma}[16,569 - 2(29,182\sqrt{\gamma} + 17,937\gamma - 383,610\gamma^{3/2} \\
&\quad - 489,213\gamma^2 + 17,118,900\gamma^{5/2} - 99,959,670\gamma^3 + 321,418,800\gamma^{7/2} - 656,219,340\gamma^4 \\
&\quad + 886,243,680\gamma^{9/2} - 761,934,600\gamma^5 - 116,575,200\gamma^{11/2} + 1,784,008,800\gamma^6 \\
&\quad - 1,494,158,400\gamma^{13/2} + 2,947,492,800\gamma^7)]\}, \\
q_2 &= -28\gamma(793 - 4887\sqrt{\gamma} + 2356\gamma + 45,582\gamma^{3/2} - 47,816\gamma^2 - 705,198\gamma^{5/2} \\
&\quad + 666,780\gamma^3 + 24,815,220\gamma^{7/2} - 135,485,460\gamma^4 + 247,556,520\gamma^{9/2} + 22,090,320\gamma^5 \quad (35) \\
&\quad - 648,058,320\gamma^{11/2} + 1,087,732,800\gamma^6 - 4,951,497,600\gamma^{13/2} - 2,471,212,800\gamma^7 \\
&\quad - 5,753,462,400\gamma^{15/2} - 6,921,028,800\gamma^8), \\
q_3 &= -28(190\sqrt{\gamma} - 504\gamma - 2604\gamma^{3/2} - 2151\gamma^2 + 63,736\gamma^{5/2} - 394,206\gamma^3 \\
&\quad + 948,840\gamma^{7/2} + 1,008,690\gamma^4 + 11,324,880\gamma^{9/2} - 42,689,700\gamma^5 - 43,133,040\gamma^{11/2} \\
&\quad + 530,583,480\gamma^6 + 1,034,661,600\gamma^{13/2} + 3,690,262,800\gamma^7 + 6,280,545,600\gamma^{15/2} \\
&\quad + 6,643,425,600\gamma^8 + 7,919,856,000\gamma^{17/2} + 3,510,864,000\gamma^9), \\
q_4 &= -28[1 - 5\gamma(2 + 15\sqrt{\gamma} + 40\gamma + 60\gamma^{3/2} + 96\gamma^2 + 60\gamma^{5/2})](19 \\
&\quad - 18\gamma\langle 7 - 3\gamma\{4 - 35\sqrt{\gamma}(1 + 2\gamma)[8 - 3\gamma(111 + 416\sqrt{\gamma} + 190\gamma)]\}\rangle), \\
r_0 &= 2\gamma(3 - 15\sqrt{\gamma} + 40\gamma - 60\gamma^{3/2} + 60\gamma^2 - 60\gamma^{5/2}), \\
r_1 &= \sqrt{\gamma}\{3 - 10\gamma[1 - 12\gamma(1 + 2\gamma)]\}, \\
r_2 &= 1 - 10\gamma^{3/2}[3 + 4(2\sqrt{\gamma} + 3\gamma + 3\gamma^{3/2} + 3\gamma^2)], \\
s_0 &= 2\gamma[140 - 9\sqrt{\gamma}(140 - 520\sqrt{\gamma} + 70\gamma + 8862\gamma^{3/2} - 47,355\gamma^2 \\
&\quad + 131,880\gamma^{5/2} - 215,460\gamma^3 + 224,280\gamma^{7/2} - 243,180\gamma^4)], \quad (36) \\
s_1 &= \sqrt{\gamma}[133 - 18(28\sqrt{\gamma} - 3\gamma - 28\gamma^{3/2} - 2436\gamma^2 + 21,672\gamma^{5/2} \\
&\quad - 75,600\gamma^3 + 124,320\gamma^{7/2} + 40,320\gamma^4 + 161,280\gamma^{9/2} + 362,880\gamma^5)], \\
s_2 &= 19 - 18\gamma\langle 7 - 3\gamma\{4 - 35\sqrt{\gamma}(1 + 2\gamma)[8 - 3\gamma(111 + 416\sqrt{\gamma} + 190\gamma)]\}\rangle).
\end{aligned}$$

While lengthy, the above formulae can be programmed in a spreadsheet to give rapid estimation of the lateral-torsional buckling load over a wide range of γ and small values of A , B , e , and κ^2 . It can be shown that the sensitivities with respect to A , B , e , and κ are all within 9% of the exact values (i.e., those in Eq. (21)) for small γ . For $\gamma < 0.1$, the errors on the sensitivities increase dramatically if the assumed mode does not contain an exponential term. To the authors' knowledge, sensitivities for large γ have not been published. Comprehensive validation of this formula by numerical solutions is now presented.

4. Results

The results of comparing a numerical solution of the exact perturbation equations, Eq. (6), with the results from our buckling load formula, Eq. (29), are presented in Figs. 4–14. In all cases, the approximate solutions are depicted as dashed lines, and the numerical solutions of the exact perturbation equations are

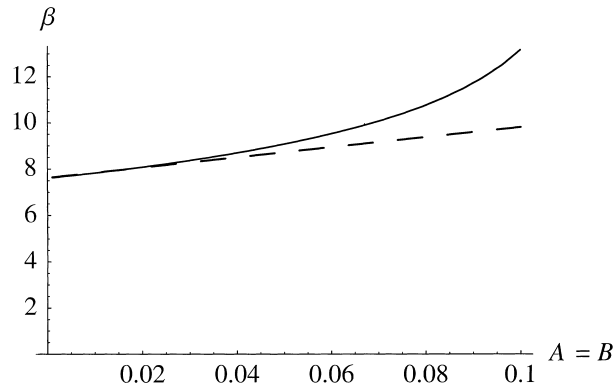


Fig. 4. Buckling load versus $A = B$ for $e = 0$, $\kappa = 0$, and $\gamma = 0.1$; solid line is numerical solution of exact equations, and dashed line is Eq. (29).

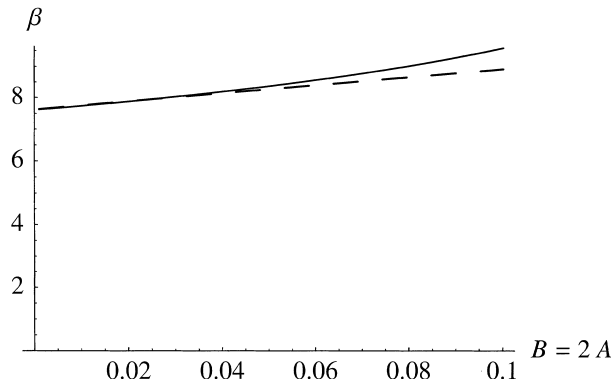


Fig. 5. Buckling load versus $B = 2A$ for $e = 0$, $\kappa = 0$, and $\gamma = 0.1$; solid line is numerical solution of exact equations, and dashed line is Eq. (29).

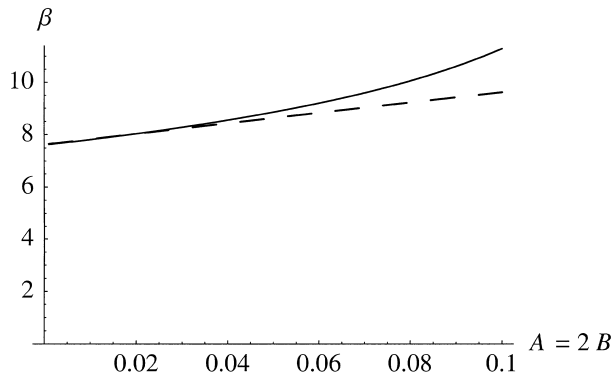


Fig. 6. Buckling load versus $A = 2B$ for $e = 0$, $\kappa = 0$, and $\gamma = 0.1$; solid line is numerical solution of exact equations, and dashed line is Eq. (29).

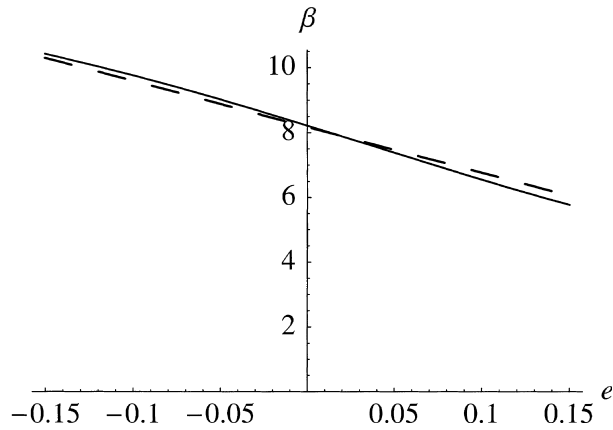


Fig. 7. Buckling load versus e for $A = 0.025$, $B = 0.025$, $\kappa = 0$, and $\gamma = 0.1$; solid line is numerical solution of exact equations, and dashed line is Eq. (29).

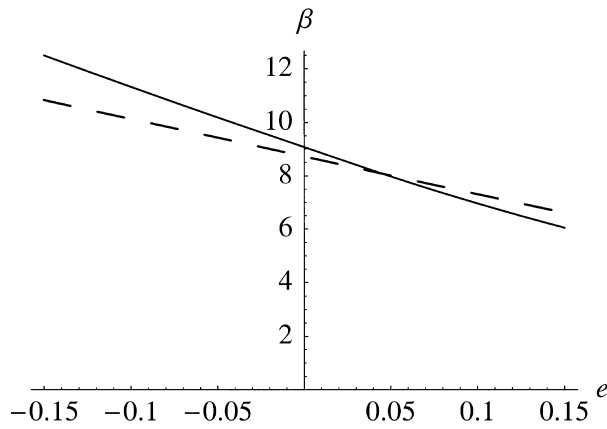


Fig. 8. Buckling load versus e for $A = 0.05$, $B = 0.05$, $\kappa = 0$, and $\gamma = 0.1$; solid line is numerical solution of exact equations, and dashed line is Eq. (29).

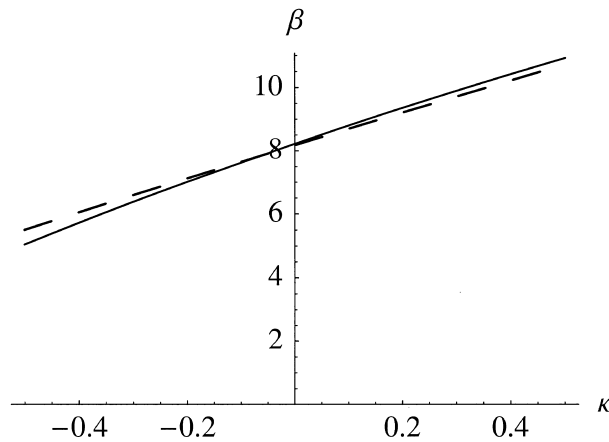


Fig. 9. Buckling load versus κ for $e = 0$, $A = 0.025$, $B = 0.025$, and $\gamma = 0.1$; solid line is numerical solution of exact equations, and dashed line is Eq. (29).

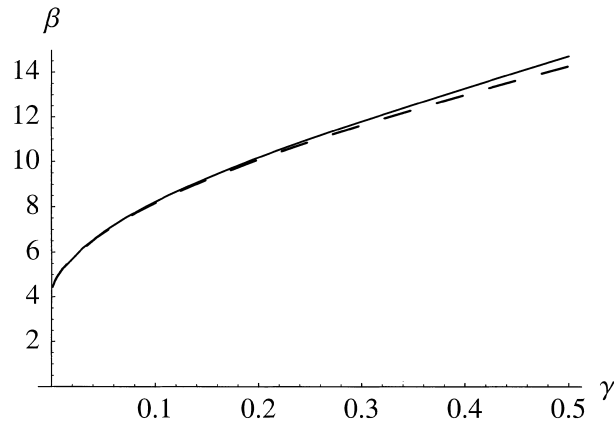


Fig. 10. Buckling load versus γ for $e = 0$, $A = 0.025$, $B = 0.025$, and $\kappa = 0$; solid line is numerical solution of exact equations, and dashed line is Eq. (29).

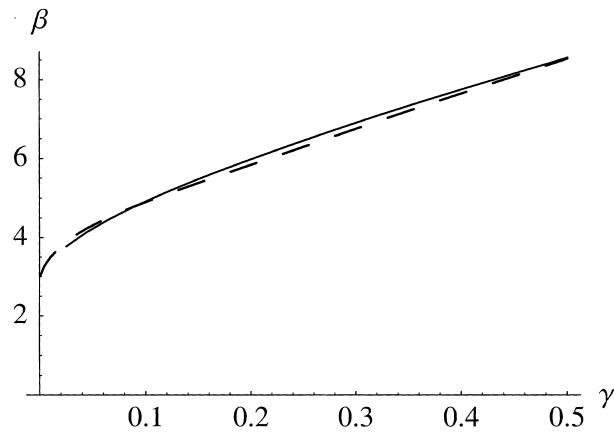


Fig. 11. Buckling load versus γ for $e = 0.1$, $A = 0.0125$, $B = 0.025$, and $\kappa = -0.2$; solid line is numerical solution of exact equations, and dashed line is Eq. (29).

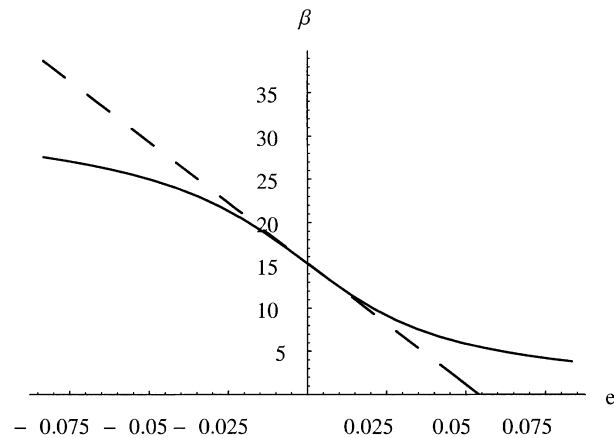


Fig. 12. Plot of β versus e for composite I-beam of Pandey et al. (1995) with ply angle of 0° ; solid line is numerical solution, and dashed line is from Eq. (29).

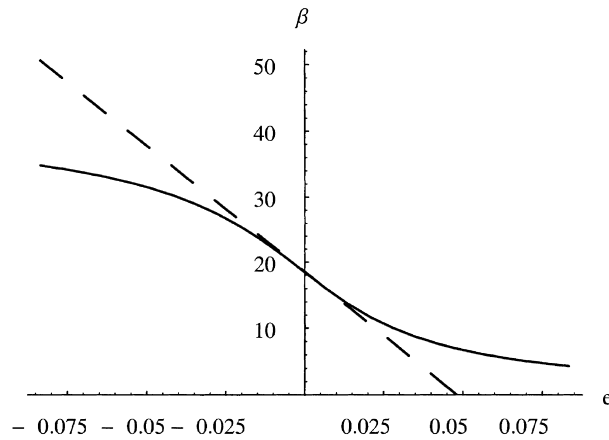


Fig. 13. Plot of β versus e for composite I-beam of Pandey et al. (1995) with ply angle of 45° ; solid line is numerical solution, and dashed line is from Eq. (29).

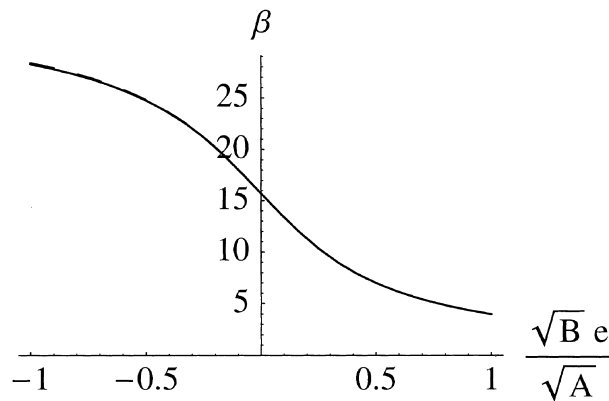


Fig. 14. Plot of β versus $e\sqrt{B/A}$ for an I-beam with $\gamma = 1$, ignoring prebuckling deflections; solid line is from the numerical solution of Eq. (37), and dashed line (nearly coincident) is from minimum over α of L (Eq. (39)) with $\phi = \theta$ from Eq. (38).

solid lines. As expected, the results indicate that the buckling load formula is very accurate when A , B , and e are small. The formula captures the behavior of the exact solution very well for all values of γ , which must be positive, and for all values of κ such that $-\frac{1}{2} < \kappa < \frac{1}{2}$, which is its range of practical values.

In Figs. 4–6, the effect of prebuckling deflections on the buckling load is shown. This effect was shown by Hodges and Peters (1975) to be reflected in the parameters A and B . Very good agreement is obtained at small values of A and B , regardless of the ratio of A to B . The worst case is when $A = B$, the buckling load formula tends to capture the behavior well for A and B less than about 0.035. At larger values of A and B , one finds a steady departure of the results from the formula away from the numerical solution with the error being conservative. It should be noted that as the buckling load increases significantly for larger A and B , these cases tend to become of less practical significance.

In Figs. 7 and 8, the variation of the buckling load with the offset of the load, e , is shown for small and moderately large values of A and B . For the values of A and B within the applicable range (i.e., <0.035), the behaviors for both positive and negative values of e are picked up well by the formula. When the values of A and B are increased, not only is there a slight disagreement at small e , but also the slope of

the curve becomes further away from the correct value. This indicates that one can use the formula even for cases in which A and B are slightly outside the formula's range of applicability. In doing so, however, one should expect that the sensitivities (as indicated by the slope of this curve) may also exhibit increased errors.

In Fig. 9, we look at the effect of elastic coupling. It is shown that bending-torsion coupling can *strongly* affect the buckling load, either positively or negatively. The behavior with κ appears to be nearly linear for this case. However, one cannot conclude that the κ^2 terms in the formula are not needed. It is clear that elastic coupling could be used to tailor the structure to have a larger buckling load without changing the bending or torsional stiffnesses.

In Figs. 10 and 11, the effects of the Vlasov term are depicted, with zero and nonzero values of all other parameters, respectively. There is very little error in the formula associated with this effect for reasons pointed out above in connection with the exponential term in the comparison function. In Fig. 11, the results for a typical case with nonzero values for all parameters are shown. There is no significant difference between the results from Eq. (29) and the numerical solution of the exact perturbation equations, Eqs. (6).

For I-beams as well as for the strip-beam, when $e\sqrt{B/A}$ is not small of the same order as A , the above approximate solution breaks down. For I-beams, however, the value of $\sqrt{B/A}$ can be large for two different reasons. First, just as for strip-beams, the effective G/E can be small for anisotropic I-beams causing A to be smaller than B . Second, even for isotropic I-beams, B/A can be large because the flange width is typically larger than the wall thickness. This means that the effect of load offset for composite I-beams can be *much* more significant than for isotropic strip-beams. To see this more clearly, we consider the composite beam example presented by Pandey et al. (1995). Results obtained therein will also be compared with the present results.

The I-beam has a uniform wall thickness of 0.00953 m, a depth of 0.2032 m, and a flange width of 0.1016 m. The length considered here is $l = 1.2192$ m. In the undertaking of this comparison, the following difficulties were encountered. First, the 3-D elastic constants for the material system considered in Pandey et al. (1995) were not given directly. Only the fiber and matrix properties were given, along with the statement that the fiber volume fraction was taken to be 60%. No statement was given as to which model was used to obtain the 3-D elastic constants, nor was their actual value given. By comparison with their results, however, it was ascertained that the simple strength of material model was used. This gives elastic constants of $E_{11} = 42.7 \times 10^9$ N/m², $E_{22} = 8.02 \times 10^9$ N/m², $G_{12} = 3.10 \times 10^9$ N/m², and $\nu_{12} = 0.248$.

The second difficulty was that the plots of torsional rigidity D_{11} , bending stiffness D_{22} , and warping rigidity D_{44} in Pandey et al. (1995) are at variance with those obtained from the asymptotically correct formulation of Volovoi et al. (1998) as well as with the basic physics of the problem. The I-beam considered was such that the upper and lower flanges were unidirectional with 0° ply angle. Only the web contained off-axis fibers, being basically a single layer of material with ply angle θ . As the web does not contribute to the smallest bending rigidity, it should not be a function of ply angle. This is not at all reflected in the plots of D_{22} and D_{44} in Pandey et al. (1995). For both these elastic constants, the asymptotic analysis shows them to be constant with ply angle, as expected, with values of $D_{22} = 71,200$ N m² and $D_{44} = 735$ N m⁴. Although our values for these constants at 0° ply angle are very close to theirs (see their Fig. 9), they show both D_{22} and D_{44} to be sharply decreasing from their maximum values at 0° ply angle to very small values at a ply angle of 90°. It is also noted that the units given by Pandey et al. (1995) are incorrect for D_{44} , the correct units being N m⁴ rather than kN m.

Finally, Pandey et al. (1995) show the torsional rigidity, D_{11} , on the same plot as D_{22} , reaching a maximum value at a ply angle of 45°. However, the results from the asymptotic analysis for D_{11} are three orders of magnitude smaller than theirs; moreover, from the asymptotic analysis the correct peak value is not nearly as large relative to the 0° ply angle value as the one they obtained. For ply angle of 0°, we obtain $D_{11} = 364$ N m², and for ply angle of 45°, we obtain $D_{11} = 610$ N m². For completeness, we note that for 0° ply angle $D_{33} = 1.14 \times 10^6$ N m² and for ply angle of 45°, we get $D_{33} = 912,000$ N m².

The cases with ply angles of 0° and 45° are chosen for presentation here. For both cases $\kappa = 0$; indeed, we have found it difficult to conceive of an I-beam configuration which will yield a large value of κ . For the case with ply angle equal to 0° , the nondimensional constants are $A = 0.000319$, $B = 0.0625$, and $\gamma = 1.36$. For the case with ply angle of 45° , $A = 0.000669$, $B = 0.0780$, and $\gamma = 0.810$. The sensitivity with respect to e is large for both cases because of the large values of $\sqrt{B/A}$, resulting in highly nonlinear behavior of β relative to e as shown in Figs. 12 and 13. The results from Eq. (29) are shown for reference. As with the strip-beam, when $\sqrt{B/A}$ is large, one must *not* expect the linear trend with respect to e to be valid. The buckling load formula does give, however, accurate predictions of the buckling load at small e and of the slope of the curve at $e = 0$.

Given the significant discrepancies in the cross-sectional constants used by Pandey et al. (1995), one should not expect our results to be in agreement with theirs. At 0° ply angle, their results give a buckling load of approximately 72,000 N, versus 63,500 N from our analysis. At 45° , they obtained 54,000 N, whereas ours results give 67,500 N. Indeed, not only are the numerical values very different; more significantly, the trend versus ply angle is the opposite. Their results are maximum at 0° , while ours peak at 45° ; their results are minimum at 45° but ours at 0° . From the above discussion of the section properties, there are significant reasons to believe that the results presented by Pandey et al. (1995) are incorrect. On the other hand, although we do not have any results from a truly independent approach to validate ours (such as 3-D finite elements), we have several good reasons that suggest the present results are correct: the well-validated asymptotic formulae used for the section constants, the trends in these constants following the expected behavior, and the excellent agreement between our formula and an essentially exact numerical solution.

Accurate treatment of the cases where $e\sqrt{B/A}$ is not small compared to unity is far more problematic. Somehow one must remove the restriction that e is a small parameter, because it always appears multiplied by $\sqrt{B/A}$ in the boundary conditions. Alternatively, it could mean treating A as a much smaller parameter than all others. Proceeding as above with these kinds of changes would make the already long formulae above far more complicated. For the case in which all prebuckling deflections are ignored, an alternative approach, based on the treatment of Rayleigh's quotient with a free parameter in Hodges (1997), can be developed as follows:

The governing equation is the same as Eq. (24), but with a different boundary condition at the free end, viz.,

$$\begin{aligned} \gamma\phi'''' - \phi'' - x^2\beta^2\phi &= 0, \\ \phi(1) = \phi'(1) = \phi''(0) = \gamma\phi'''(0) - \phi'(0) - \frac{\sqrt{B}e\beta\phi(0)}{\sqrt{A}} &= 0. \end{aligned} \quad (37)$$

The simplest possible admissible function that satisfies the first three boundary conditions and contains both the exponential term and a free parameter is used, given by

$$\theta = -(1-x)^2e^{-1/\sqrt{\gamma}} + 2(1-x)\sqrt{\gamma} + 2\gamma e^{-(1-x)/\sqrt{\gamma}} - 2\gamma[1 - \alpha(2 - 3x + x^3)]. \quad (38)$$

The energy functional depends on ϕ and its derivatives and is of the form

$$L = \frac{1}{2} \int_0^1 (\gamma\phi'^2 + \phi'^2 - \beta^2x^2\phi^2) dx - \frac{\sqrt{B}e\beta\phi^2(0)}{2\sqrt{A}}. \quad (39)$$

One first substitutes $\phi = \theta$ into L , then minimizes L with respect to α , and finally solves the resulting quartic equation for β . This yields a closed-form approximate formula for the buckling load. Although it is a very complicated expression (too long to print here), it is not too difficult for computerized symbolic manipulation to handle. Results from this approximate closed-form expression for the buckling load are compared with a numerical solution of Eq. (37) in Fig. 14. The agreement is excellent. To add the prebuckling de-

flections may present difficulties for some symbolic computational tools. However, as shown above, these effects generally make the predicted buckling load larger and frequently may be ignored for design purposes.

5. Conclusion

The geometrically exact elastica equations for a composite beam are applied to the lateral–torsional buckling analysis of an end-loaded composite cantilever beam. Considering the case for which the pre-buckling state is planar deformation, a stability analysis was developed based on the equations, linearized about the prebuckling state. Moreover, consistently ignoring terms of the order of the square of the pre-buckling section rotation compared to unity in both the prebuckling and perturbation equations, one obtains a single ordinary differential equation that governs the stability problem. Using the energy method and a single comparison function for the beam without any of the small terms, an approximate closed-form expression for the buckling load was written which takes into account various refinements of previously published results, including the Vlasov effect, elastic coupling, the offset of the load from the centroid, and, of course, prebuckling deflections. This formula, then, can be used with confidence, in conjunction with published asymptotically correct stiffness constants of composite I-beams and strip-beams. Indeed, it is shown herein that this formula produces results which, except for the variation of one parameter, agree quite well with a numerical solution of the exact equations. This exception involves the offset of the load from the cross-sectional centroid. This offset is normally small relative to the beam length, so that the ratio can be treated as a small parameter. However, its only appearance is in the boundary conditions where it is multiplied by a quantity which can be large for composite strip-beams and for I-beams in general. Thus, the offset cannot be treated as a small parameter in those cases. To deal with the exception, a separate development that ignores the (normally small) effects of prebuckling deflections is presented, yielding a formula that matches with the exact solution very well for that case.

References

- Bauld Jr., N.R., Tzeng, L.-S., 1984. Vlasov theory for fiber-reinforced beams with thin-walled open cross sections. *International Journal of Solids and Structures* 20, 277–297.
- Hodges, D.H., 1990. A mixed variational formulation based on exact intrinsic equations for dynamics of moving beams. *International Journal of Solids and Structures* 26, 1253–1273.
- Hodges, D.H., 1997. Improved approximations via Rayleigh's quotient. *Journal of Sound and Vibration* 199, 155–164.
- Hodges, D.H., Peters, D.A., 1975. On the lateral buckling of uniform slender cantilever beams. *International Journal of Solids and Structures* 11, 1269–1280.
- Michell, A.G.M., 1899. Elastic stability of long beams under transverse forces. *Philosophical Magazine* 48, 298–309.
- Pandey, M., Kabir, M., Sherbourne, A., 1995. Flexural–torsional stability of thin-walled composite I-section beams. *Composites Engineering* 5, 321–342.
- Prandtl, L., 1899. *Kipperscheinungen*. Doctoral dissertation, Universität München.
- Reissner, E., 1979. On lateral buckling of end-loaded cantilever beams. *Journal of Applied Mathematics and Physics* 30, 31–40.
- Reissner, H., 1904. Über die Stabilität der Biegung. *Sitz.-Ber. der Berliner Mathem. Gesellschaft*, III. Jhg., 53–56. Beilage zum Archiv der Mathem. u. Physik.
- Timoshenko, S.P., Gere, J.M., 1961. *Theory of Elastic Stability*. Second edition. McGraw-Hill, New York.
- Volovoi, V.V., Hodges, D.H., Berdichevsky, V.L., Sutyurin, V., 1998. Asymptotic theory for static behavior of elastic anisotropic I-beams. *International Journal of Solids and Structures* 36, 1017–1043.